

Comparison of the Oxidation Behaviors of High FeO Chromite and Magnetite Concentrates Relevant to the Induration of Ferrous Pellets



DEQING ZHU, CONGCONG YANG, JIAN PAN, and XIAOBO LI

Oxidation process plays an important role in producing sufficiently strong ferrous pellets for blast furnace, and the oxidation behavior of pellet feed greatly affects the quality of pellets. As a supplementary research to earlier published work, the present study fixes its particular attention on the fundamental oxidation behavior of a high FeO South African chromite concentrate in comparison to that of typical magnetite concentrate using differential scanning calorimetry, X-ray diffraction analysis, and thermogravimetry at various temperatures ranging from 473 K to 1273 K (200 °C to 1000 °C). The reaction mechanism and phase transformation during the oxidation process of chromite spinel is further explained by thermodynamics calculation performed by FactSage software. Besides, routine laboratory preheating–roasting test of single ore pellets is also conducted to reveal the relevance of oxidizability to the consolidation of pellets. The results show that the chromite spinel possesses much poorer oxidizability than magnetite, usually accompanying complex phase transformations *via* a preferential nucleation of Fe-rich sesquioxide from the chromite spinel matrix at low temperatures and thereafter the formation of Cr-rich sesquioxide on the substrate of Fe-rich phase at high temperatures. The oxidation of chromite spinel is inferior to that of magnetite from the viewpoint of thermodynamics and dynamic kinetics. Good inherent oxidizability of raw materials is found to have a positive effect on the induration process of pellet.

DOI: 10.1007/s11663-016-0770-2

© The Minerals, Metals & Materials Society and ASM International 2016

I. INTRODUCTION

WITH the increasing depletion of high grade chromite ores, especially for “lumpy ores,” pioneering endeavor that aims at reducing the production cost and promoting the competitiveness of stainless steel products in the market now is carried out by utilizing cost-effective chromite fines or concentrates with low $\text{Cr}_2\text{O}_3/\text{FeO}$ ratio.^[1,2] In an earlier study, pelletization of high FeO South African chromite concentrates with coexistence of domestic magnetite concentrates for a novel blast furnace (BF) smelting process was investigated and the consolidation mechanism of oxidized pellets was revealed.^[3,4] It was found that the non-fluxed chromite–magnetite composite pellets were predominantly solid-state bonded relying on the recrystallization of hematite and formation of solid solutions in adjacent areas of both chromite–magnetite and chromite–chromite particles, which are largely affected by the oxidizability of chromite and magnetite spinels. However, the oxidation behaviors of high FeO chromite concentrates

in relation to the hardening of pellets have not been well investigated.

It has been stressed that oxidation of magnetite is extremely important to the induration of pellets only when a defective structure occurs and then undergoes phase transformation at higher temperatures, resulting in more efficient consolidation.^[5–7] Generally, oxidation of both magnetite and chromite spinels to sesquioxides in air follows a two-stage process.^[8–11] It begins with the oxidation of ferrous spinels to an intermediate defect phase (known as the gamma phase with a spinel structure, in which a certain amount of vacancies locate on the octahedral and tetrahedral sites) at low temperature and then transforms to stable alpha phase with a corundum structure when temperature increases to a higher level. However, with increasing substitution of cations like Cr^{3+} , Mg^{2+} , Al^{3+} , and Ti^{4+} for Fe^{2+} , Fe^{3+} ions in magnetite crystal structure, ideally as pure ferrous spinels or natural complex chromite spinels $(\text{Fe}^{2+}, \text{Mg}^{2+})[\text{Cr}^{3+}, \text{Fe}^{3+}, \text{Al}^{3+}, \text{Ti}^{4+}]_2\text{O}_4$, the spinel structure tends to be stabilized and moreover, both oxidation of spinel phase to metastable γ -phase and its transition to stable α -phase are found to shift to higher temperatures.^[4,12–18] The discrepancy of oxidation behaviors will inevitably affect the hardening of oxidized pellets.

In this work, particular attention was fixed on the comparison of oxidation behaviors of high FeO chromite and magnetite concentrates in relation with the hardening of their pellets. A set of methods, for example differential scanning calorimetry (DSC),

DEQING ZHU, Professor, CONGCONG YANG, Ph.D. Student, JIAN PAN, Associate Professor, and XIAOBO LI, Graduate Student, are with the School of Minerals Processing and Bioengineering, Central South University, Changsha, 410083, P.R. China. Contact e-mails: smartyoung@csu.edu.cn, ccy-patrickyoung@hotmail.com

Manuscript submitted December 20, 2014.

Article published online August 4, 2016.

thermogravimetric analysis (TG), X-ray diffraction (XRD), thermodynamic calculations performed by FactSage software, were used to reveal the mechanism and kinetics of oxidation process. In addition, the compressive strength and microstructure of chromite and magnetite pellets are also studied.

II. EXPERIMENTAL

A low grade chromite concentrate from South Africa with a $\text{Cr}_2\text{O}_3/\text{FeO}$ of 1.99 is chosen as raw material from the viewpoint of its good economics and abundant reserves for sustainable production.^[1,19] In the meantime, a typical and widely used magnetite concentrates from northeastern China is adopted for comparison. The chemical compositions of the samples determined by chemical titration method was given in Table I and their phase compositions by XRD analysis are shown in Figure 1. It can be known from Table I that the FeO contents in chromite and magnetite concentrates are 21.38 and 27.67 pct, respectively. The XRD patterns indicate that the main mineral phase in chromite concentrate is in the form of spinel phase, $(\text{Fe, Mg})[\text{Cr, Al, Fe}]_2\text{O}_4$, and the main mineral phase in magnetite concentrate is in Fe_3O_4 form.

A. Thermal Analysis

Thermal analysis, including DSC and TG analysis were conducted in a NETZSCH STA449C thermal analyzer. In each experiment, 15 mg powdered sample (-0.045 mm) was placed in an alumina crucible and then tested in the analyzer at an isochronal heating rate of 10 K/min. During the whole process, air was chosen as the testing atmosphere and the gas flow rate was set at a specific value of 70 mL/min by applying conventional testing procedure.^[20] The DSC-TG experiments of each sample will be repeated three times under a standard deviation of ± 3 pct to acquire good reproducibility of the results. The differential thermogravimetric analysis (DTG) data were obtained by the first-order differential calculation from the TG data.

B. Phase Analysis

The samples for phase transformation study were prepared by isochronal preheating of the chromite and magnetite concentrates separately at different temperatures in an electrical tube furnace that interlinked with the open air. The preheated samples were subsequently cooled in the nitrogen atmosphere. The heat treatment procedure in the furnace equipment had been reported

in author's research.^[21] A range of temperatures from 473 K to 1273 K (200 °C to 1000 °C) at an interval of 50 K and 100 K were tested and the preheating duration was 10 minutes at each temperature based on common industrial practice.

A Rigaku D/max 2550 X-ray diffractometer using copper target (40 KV, 250 mA) was applied for phase analysis and the continuous scanning range was from 5 to 70 deg at a rate of 4 deg per minute. Before testing, the peak positions will be calibrated after scanning standard sample $\alpha\text{-SiO}_2$. The MDI/Jade 9 software was used for phase searching and analyzing. Specific peak positions at (220) plane of spinel phases and (104) plane of sesquioxides (including hematite) were captured from the XRD patterns to reveal phase transformations. Thermodynamic calculations of $\text{Cr}_2\text{O}_3\text{-Fe}_2\text{O}_3\text{-Al}_2\text{O}_3$ ternary system in air from 673 K to 1273 K (400 °C to 1000 °C) were performed by FactSage software to interpret the formation mechanism of sesquioxide solid solutions.

C. Oxidation Kinetics of Chromite and Magnetite Pellets

The oxidation kinetics of chromite and magnetite were determined in pellet form in a vertical furnace by thermogravimetric method. The reaction apparatus could also be found elsewhere in other researches.^[5,22-24] The chromite and magnetite concentrates were prepared to bear similar particle size distribution and SSA value, as shown in Table II. The two concentrates were then pelletized with water in a laboratory disk pelletizer

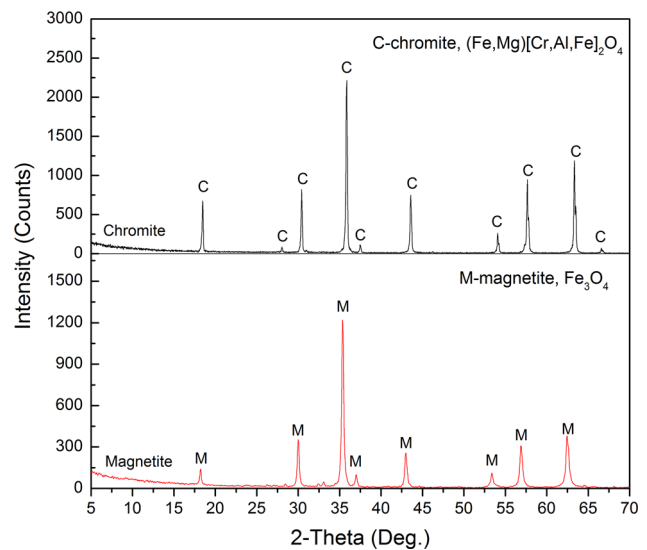


Fig. 1—XRD patterns of chromite and magnetite concentrates.

Table I. The Chemistry of Iron Ore Concentrates (Mass Pct)

Sample	Fe _{Total}	FeO	Cr ₂ O ₃	CaO	MgO	Al ₂ O ₃	SiO ₂	LOI*
Chromite	22.61	21.38	42.55	1.86	8.82	13.43	1.88	1.03
Magnetite	65.12	27.67	—	0.98	1.49	1.42	3.61	0.99

*LOI—Loss on ignition in air at 1273 K (1000 °C).

Table II. Particle Size Distributions and the SSA Values of Concentrates

Sample	Mass Fraction in Each Size (mm)			SSA Values (cm ² /g)
	+0.074	-0.074 + 0.045	-0.045	
Chromite concentrate	18.9	30.3	50.8	1105
Magnetite concentrate	19.0	23.9	57.1	1138

The SSA values are measured using Blaine method.

Table III. The Physical Parameters of Dried Pellets for Kinetics Research

Sample	Pellet Diameter (mm)	Solid Apparent Density, ρ_A (g/cm ³)	Porosity, ε (Pct)
Chromite pellets	10.8	3.12	27.3
Magnetite pellets	10.5	3.39	27.4

separately. Green pellets were manufactured by balling the concentrates for 12 minutes and then dried at 378 K (105 °C) in an oven for 4 hours. The physical parameters of two dried pellets are given in Table III.

By referring the ISO standard (ISO 4695-1995), about 100 g dried chromite or magnetite pellets were carefully loaded into a quartz tube reactor with 35 mm in diameter and 600 mm in length in each batch of experiment. Then the reactor was suspended into designated temperature zone of the vertical furnace monitored by a temperature controller within ± 5 K and heated for 10 minutes to be uniformly heated with a protection of 5 L/min high purity nitrogen, after which the nitrogen was cut off and switched to 5 L/min air. The air flow rate, 5 L/min (linear velocity = 8.66 cm/s), was determined for industrial purpose. Besides, the effect of external mass diffusion can be negligible when modified Sherwood number is over 30 or linear velocity of gas flow is over 5 cm/s.^[21,25,26] A real-time recording of weight change was conducted for 10 minutes when oxidation began. The oxidation kinetics of two types of pellets in present study was both measured in temperature range from 1073 K to 1223 K (800 °C to 950 °C), which was in the temperature range of pellet preheating in industrial operations. The oxidation extent of heated pellets, x , can be calculated by Eq. [1]:

$$\text{The oxidation extent, } x = \frac{\text{Actual weight gain at time } t}{\text{Theoretical weight gain}} \quad [1]$$

In earlier studies, a modified unreacted core shrinking model (MUCS) was usually applied to describe the oxidation kinetics of magnetite pellets by assuming that the reactions occurred at a sharp interface between the unreacted core and product layer.^[5,24] In this work, a model^[22] considering isothermal gas-porous solid reaction was applied to study the oxidation kinetics of chromite and magnetite pellets. The overall rate is given in Eq. [2].

$$t^* = g_{F_g}(x) + \hat{\sigma}^2 p_{F_p}(x), \quad [2]$$

where t^* is the dimensionless time; $\hat{\sigma}$ is the generalized gas–solid reaction modulus; $g_{F_g}(x)$, $p_{F_p}(x)$ represent

conversion functions; and F_g , F_p are the shape factors of pellets and grains, respectively ($= 1, 2$, and 3 for infinite slabs, long cylinders, and spheres, respectively).

For rate controlled by chemical reaction, $\hat{\sigma}^2$ becomes very small and Eq. [2] can be written as:

$$t^* = g_{F_g}(x) = K \cdot t \equiv 1 - (1 - x)^{1/F_g} \quad [3]$$

When overall rate is controlled by diffusion reaction through the product layer, it can be further written as:

$$t^* = K' \cdot t = p_{F_p}(X), \quad [4]$$

where $t \equiv K' \cdot [1 - 3(1 - x)^{2/3} + 2(1 - x)]$, and $F_p = 3$ in this study.

When overall rate is controlled by chemical reaction and diffusion, Eq. [2] can be given:

$$t^* \approx g_{F_g}(x) + \hat{\sigma}^2 p_{F_p}(x) \quad [5]$$

If $F_g = F_p = 3$, then Eq. [5] could be expressed as:

$$t = K_1[1 - (1 - x)^{1/3}] + K_2[1 - 3(1 - x)^{2/3} + 2(1 - x)] \quad [6]$$

The above models were used to fit the kinetic data by plotting $1 - (1 - x)^{1/F_g}$ ($F_g = 1, 2$, and 3), $[1 - 3(1 - x)^{2/3} + 2(1 - x)]$ vs time t and $1 - (1 - x)^{1/F_g}$ vs $[1 - 3(1 - x)^{2/3} + 2(1 - x)]$ successively. The best-fit model will be applied to describe the reaction and calculate the activation energy of oxidation according to the Arrhenius equation:

$$\ln k = -\frac{E_a}{R} \cdot \frac{1}{T} + \ln A, \quad [7]$$

where R is the constant, 8.314 (J/mol K), T is oxidation temperature (K), and A is the frequency factor in min^{-1} . The apparent activation energy, E_a , was calculated from the slope of linear relationship of $\ln k$ vs $1/T$ and $\ln A$ is the intercept of the line.

D. Preheating–Roasting Performance of Chromite and Magnetite Pellets

Comparison of the preheating–roasting performance of dried chromite and magnetite pellets will be conducted in the aforementioned electrical tube furnace under following conditions: preheating tests are performed at various temperatures from 473 K to 1373 K (200 °C to 1100 °C) for 10 minutes while roasting tests follows the same procedure reported in an earlier work^[4] by preheating at 1223 K (950 °C) for 10 minutes and then roasting at various temperatures from 1373 K to

1548 K (1100 °C to 1275 °C) for 12 minutes. The cold compressive strength of preheated and roasted pellets is measured and their microstructure is demonstrated under a Leica DM4500P optical microscope.

III. RESULTS AND DISCUSSION

A. Thermal Analysis of Chromite and Magnetite Concentrates

The thermal properties of chromite and magnetite concentrates are investigated and compared by employing the thermal analysis techniques including DSC, TG, and DTG.

The DSC and TG–DTG curves of two concentrates are shown in Figures 2 and 3, respectively. It can be seen

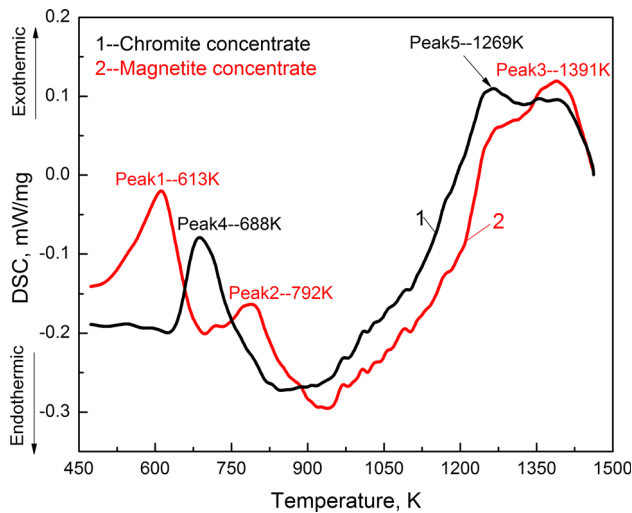


Fig. 2—DSC curves of chromite and magnetite concentrates.

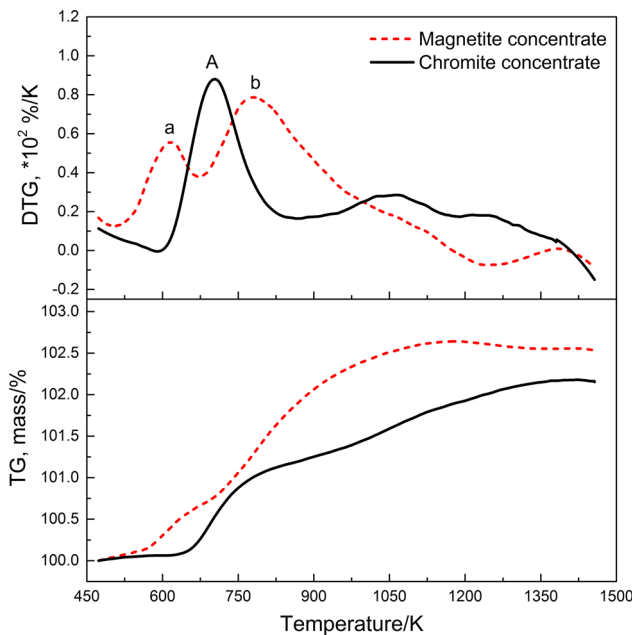


Fig. 3—TG–DTG curves of chromite and magnetite concentrates.

that the DSC curve of magnetite concentrate is characterized by twin sharp exothermic peaks (peaks 1 and 2) at 613 K and 792 K (340 °C and 519 °C), respectively, which are followed by a broad exothermic peak (peak 3) beginning at 923 K (650 °C) and having a maximum peak temperature of about 1391 K (1118 °C). Correspondingly, the TG curve shows initial weight gain that begins at 473 K (200 °C) due to the oxidation of magnetite and the maximum weight gain that appears at around 1173 K (900 °C), indicating the completion of oxidation process. In contrast, the DSC curve of chromite concentrate only has a sharp exothermic peak (peak 4) at 688 K (415 °C) and is also followed by a broad exothermic peak (peak 5) beginning at around 873 K (600 °C) and having a maximum peak temperature of around 1265 K (992 °C). The oxidation of chromite seems to be more difficult than that of magnetite since its weight gain begins at a higher temperature of 673 K (400 °C) and subsequently undergoes a slow oxidation process until a maximum weight gain occurs at approximately 1373 K (1100 °C). The DTG curves of both magnetite and chromite concentrates exhibit similar peak positions with their corresponding exothermic peaks on DSC curves.

Considerable differential thermal studies on the oxidation of magnetite have been conducted previously but leaving a controversial topic because of quite a number of published contradictions regarding the interpretation of the exothermic peaks on the DTA (or DSC) curve, especially the early twin peaks at low temperatures. Both Schmidt^[27] and Chaklader^[28] found that the intensity of first peak would decrease with the increasing particle size (or the specific surface areas) of magnetite particles and concluded that the first exothermic peak was caused by the surface oxidation while the third broaden peak in higher temperature range was a result of bulk oxidation, whereas the second exothermic peak in the temperature range of 773 K to 873 K (500 °C to 600 °C) was ascribed to the magnetic transition from ferro- to paramagnetism. A different point of view was proposed later by Gillot^[12], who attributed the formation of earlier two peaks to the oxidation of Fe^{2+} ions to a maximum extent followed by the $\gamma \rightarrow \alpha$ phase transformation. However, Sanders^[29] pointed out that the formation of gamma phase is difficult to be identified from TG and DSC curves and the second exothermic peak cannot simply be attributed to the conversion of $\gamma\text{-Fe}_2\text{O}_3$ to $\alpha\text{-Fe}_2\text{O}_3$ because of the inferior correspondence between TG–DSC data and reaction mechanisms. But he also added that the DSC data after considerable improvement does suggest the conversion of metastable to stable hematite.

Similarly, a series of investigations^[12–14] based on the differential thermal analysis and thermogravimetry on the oxidation of chromite spinel phases, *i.e.*, pure chromite spinel FeCr_2O_4 and Al-, Cr-substituted spinels $(\text{Fe})[\text{Cr}, \text{Al}, \text{Fe}]_2\text{O}_4$, have shown the evidence of $\gamma \rightarrow \alpha$ phase transformation. The conversion temperature is prone to increase with the increasing substitution of chromium and aluminum in spinel structure. Tathavakkar^[16] investigated the thermal behavior of a natural South African chromite ore bearing similar chemical

compositions to that used in the present work. He also found that there was only one single exothermic peak at about 650 K (377 °C). However, Ramos^[17] later

reported that there were two distinct sharp exothermic peaks at higher temperatures of 673 K and 1048 K (400 °C and 775 °C), respectively, on the DTA curve of

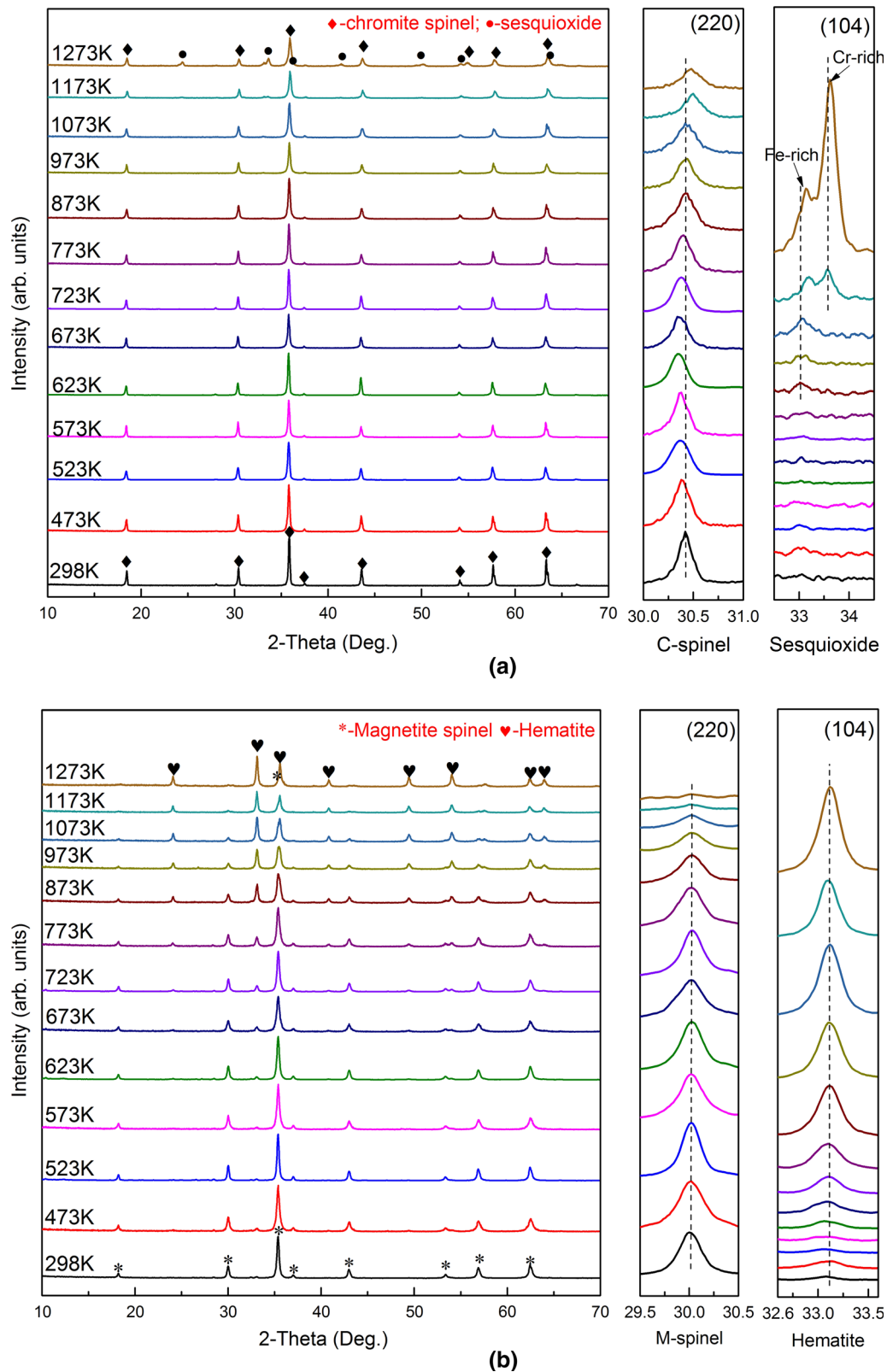


Fig. 4—XRD patterns of chromite (a) and magnetite concentrate (b) after isochronal oxidation from 473 K to 1273 K (200 °C to 1000 °C). On the right side are the (220) peaks of spinel phase and (104) peaks of sesquioxide.

another natural South African chromite ore bearing lower iron grade and higher silicate content. These previous studies are usually incompatible because of the considerable differences in physicochemical properties of raw materials and the experimental conditions (*e.g.*, heating rate) for TG-DTA study.

The above discussion has shown that magnetite is much easier to be oxidized in air than chromite. It also tells a truth that depending on TG-DSC study only may not be enough to characterize unambiguous oxidation mechanism of natural magnetite and chromite. The early exothermic peaks at low temperatures may be reflected as a combined effect of oxidation, phase, and magnetic transition while broaden exothermic peak at higher temperature may be caused by the bulk oxidation, phase transition, and the recrystallization of sesquioxide (hematite).

B. Phase Transformation During Oxidation

X-ray diffraction technique is a frequently used way in investigating the phase transformation during the oxidation of magnetite and chromite. The XRD patterns of chromite and magnetite concentrates after isochronal oxidation at various temperatures are shown in Figures 4(a) and (b). The results of phase analysis agree well with the TG-DSC study. It can be known that the sesquioxide solid solution α -(Fe, Cr, Al)₂O₃ oxidized from chromite spinel solid solution appears only when temperature is over 873 K (600 °C) while obvious characteristic peak of hematite Fe₂O₃ oxidized from magnetite spinel can be detected above 623 K (350 °C), indicating that the oxidation of chromite spinel in air is more difficult than that of magnetite.

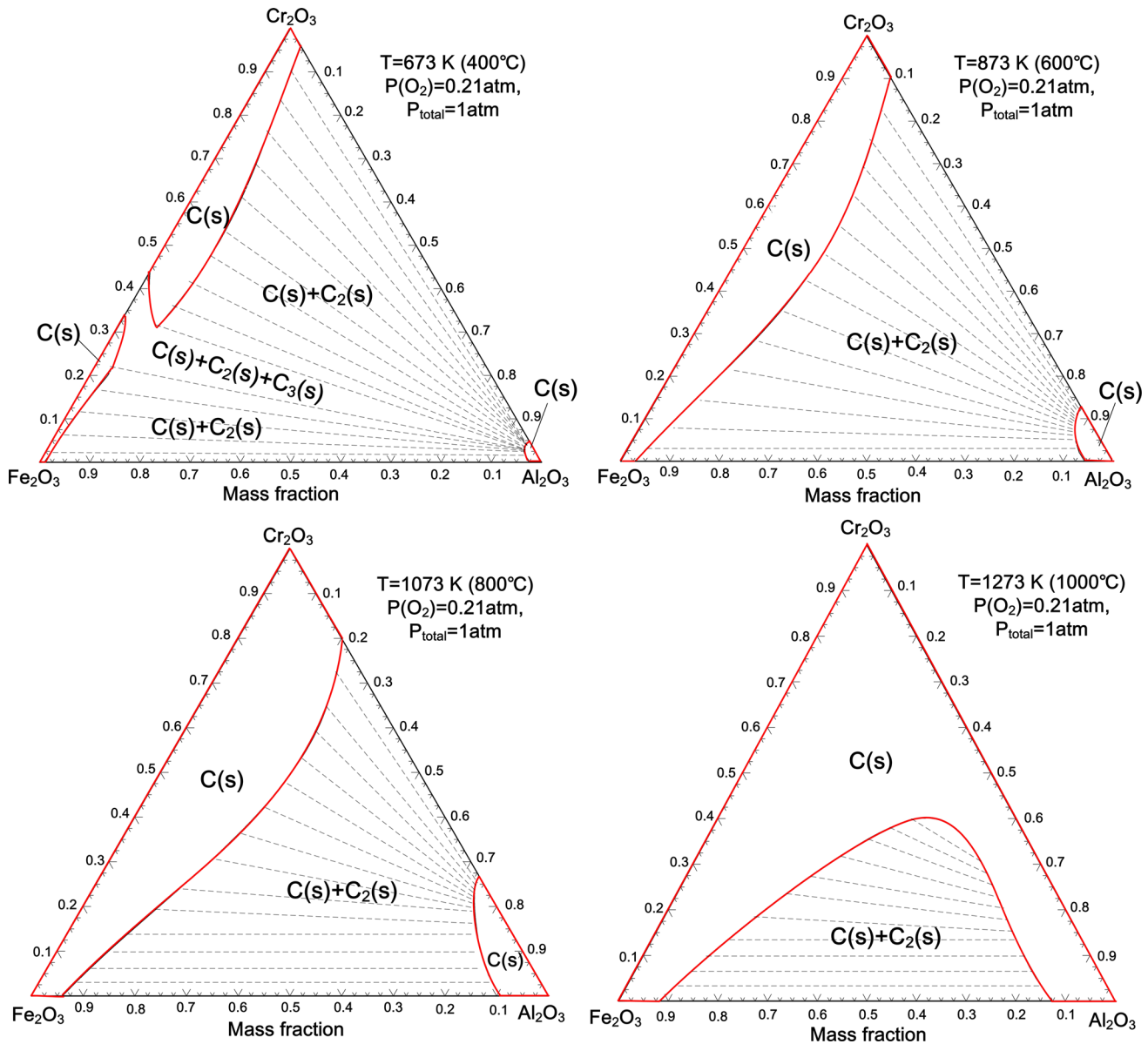


Fig. 5—Isothermal sections of Fe₂O₃-Cr₂O₃-Al₂O₃ ternary system in air from 673 K to 1273 K (400 °C to 1000 °C), labels: C-corundum; C₂-corundum 2#.

The (220) plane of spinel phases and the (104) plane of α -phases, as shown on the right side of the Figures 4(a) and (b), are selected to reveal some information about phase and structural change. As can be seen from Figure 4(a), the (220) peak position of chromite spinel phase shifts towards low diffraction angle area at first in low-temperature range of 473 K to 673 K (200 °C to 400 °C) and then moves towards high diffraction angle area when temperature is above 673 K (400 °C). Tathavadkar^[16] also reported the same observation. The cause of (220) peak shift of chromite spinel towards low and high diffraction angle area has not been clearly interpreted yet, mostly owing to the inversion or redistribution of cations.^[16,17,30] According to the classical theory of solid-state physics, the equilibrium amount of point defect (n) in solid at a specific temperature T can be expressed as:

$$n = N \cdot \exp^{-E/kT}, \quad [8]$$

where N represents the total amount of lattice points, E the Gibbs energy of defect formation, and k is the Boltzmann constant.^[31,32] It can be revealed from Eq. [8] that the equilibrium amount of defect in the spinel crystal will increase with the temperature especially in the case of quenching, which may account for the change of cell dimensions and the shift of peak positions at low temperature. The presence of point defects such as vacancy and interstitial in crystal structure is beneficial to improve diffusion and accelerate the reaction rate.^[33] When the (220) peaks of chromite spinel shift towards high diffraction angle area at over 673 K (400 °C), it implies that oxidation of Fe^{2+} ions to Fe^{3+} ions occurs corresponding to the initial weight gain on the TG curve. As both four-coordinated Fe^{3+} and Mg^{2+} ions on the tetrahedral sites have smaller ionic radius (0.049 nm for Fe^{3+} ion and 0.057 nm for Mg^{2+} ion) than that of four-coordinated Fe^{2+} ions (0.063 nm), the unit cell exhibits continuous contraction and corresponding change in (220) peak positions with the rise of temperature.

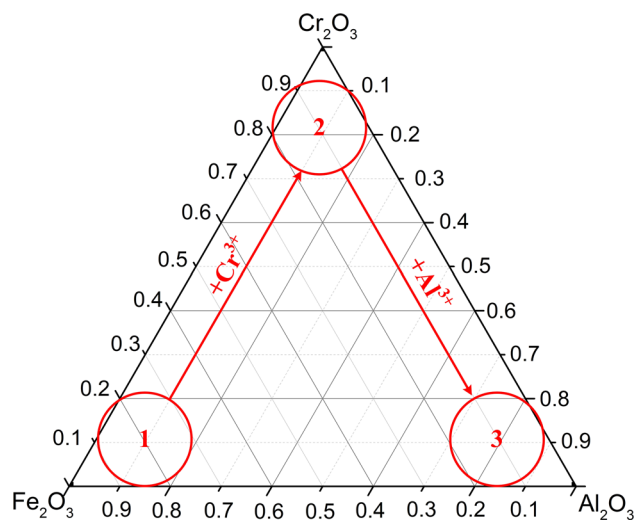


Fig. 6—Reaction sequence of Fe_2O_3 - Cr_2O_3 - Al_2O_3 ternary solid solution at elevated temperatures.

Another interesting phenomenon can be observed from the captured (104) planes of sesquioxide on the right side of Figure 4(a), in which a Fe-rich sesquioxide phase primarily forms at about 873 K (600 °C) and not until 1173 K (900 °C) a Cr-rich sesquioxide phase forms. This finding confirms the formation of a defective γ - $(\text{Fe}^{3+})[\text{Cr, Al, Fe}^{3+}]_2\text{O}_4$ spinel phase. According to Gallagher,^[34] the formation of γ -phase in spinel solid solution matrix does not require nucleation since they are virtually identical to share the same cubic crystal structure. In contrast, a nucleation process is necessary before the precipitation of α -phase because it has a different crystal structure. It was pointed out that the rate of precipitation of α - Fe_2O_3 is controlled by the degree of saturation of metastable γ -phase in the spinel matrix.^[8,34] From this point of view, the iron sesquioxide must have the lowest nucleation activation energy and is more easily precipitated from the spinel matrix, then being a perfect substrate for sesquioxide solid

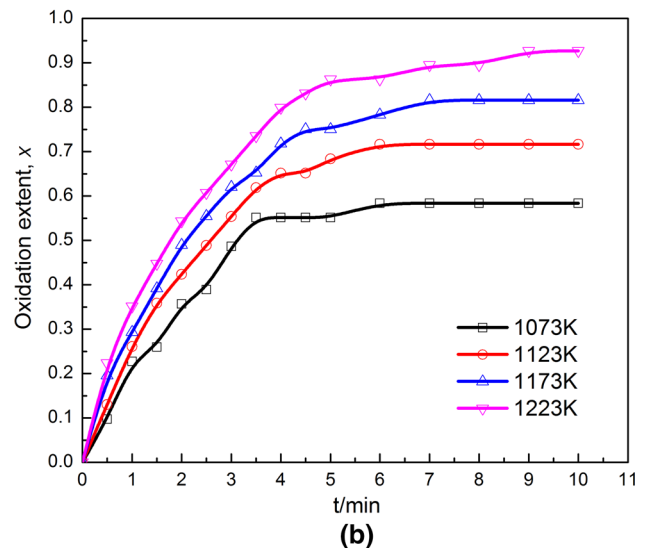
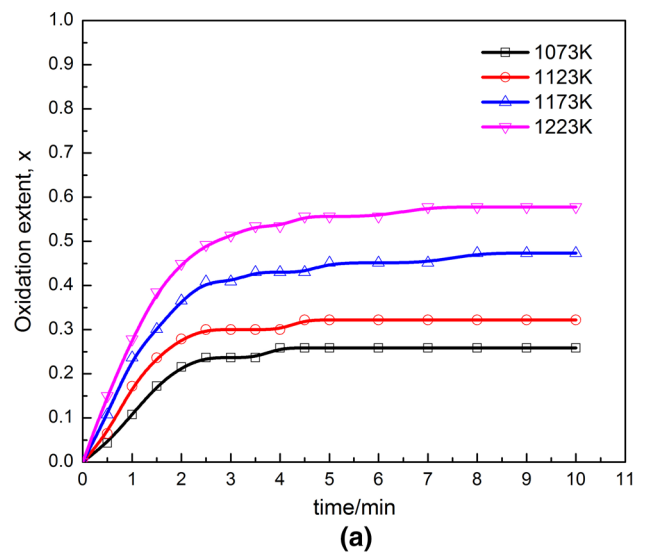


Fig. 7—Oxidation extent (x) vs time (t) curves of chromite (a) and magnetite (b) pellets in the temperature range of 1073 K to 1223 K (800 °C to 950 °C).

solution formation. And it seems reasonable to infer that the oxidation reaction of chromite spinel is controlled by nucleation of Fe-rich phase at low temperatures and diffusion of Cr^{3+} and Al^{3+} ions in solid solution at high temperatures. Figure 5 shows the

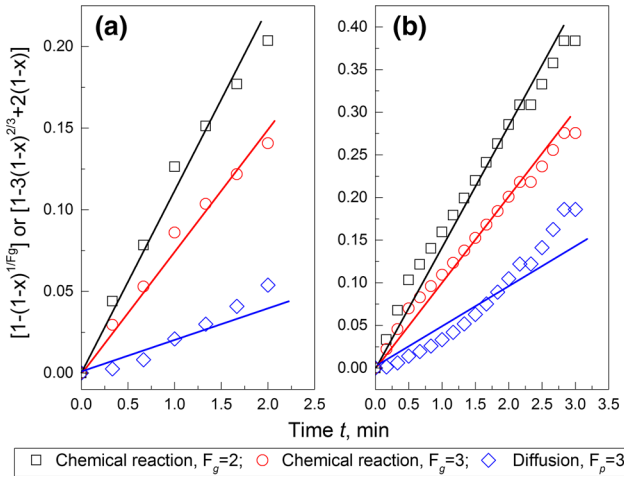


Fig. 8—Model fit of the kinetic data obtained in the oxidation of chromite (a) and magnetite pellets (b). For clarity, here only shows the plots of different functions representing rate controlled by chemical reaction or diffusion at 1173 K (900 °C).

Table IV. Reaction Rate Constant k and $\ln k$ for Two Pellets at Various Temperatures

Sample	Temperature [K (°C)]	Reaction Rate Constant, k (min^{-1})	$\ln k$
Chromite pellets	1073 (800)	0.0391	-3.241
	1123 (850)	0.0548	-2.903
	1173 (900)	0.0745	-2.597
	1223 (950)	0.0963	-2.340
Magnetite pellets	1073 (800)	0.0655	-2.725
	1123 (850)	0.0821	-2.500
	1173 (900)	0.0979	-2.324
	1223 (950)	0.1115	-2.194

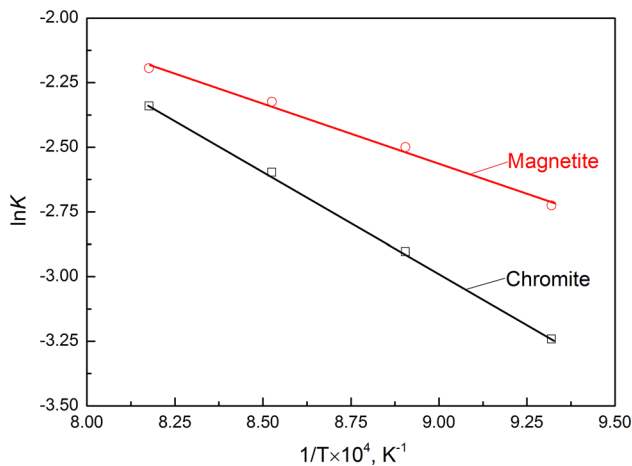
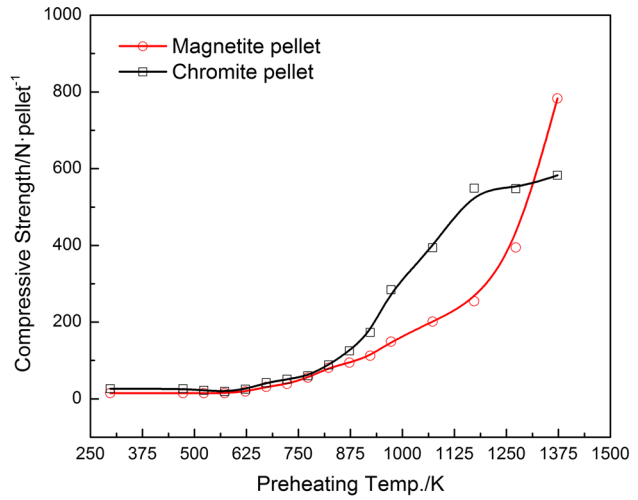


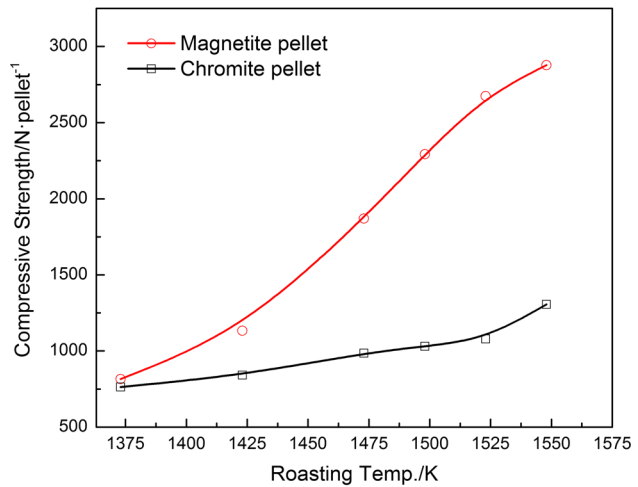
Fig. 9—Relationship between $\ln k$ and $1/T$ ($\times 10^4 \text{ K}^{-1}$) for chromite and magnetite pellets.

isothermal sections of $\text{Fe}_2\text{O}_3\text{-Cr}_2\text{O}_3\text{-Al}_2\text{O}_3$ ternary system in air from 673 K to 1273 K (400 °C to 1000 °C). The phase diagrams reveal the miscibility of three pure oxides but also show that the formation of Fe- and Cr-rich sesquioxide solid solutions is more thermodynamically supported. In association with the mentioned XRD study, the reaction sequence in spinel matrix is given in Figure 6. The preferential formation of Fe-rich sesquioxide also accounts for improving the consolidation of chromite pellets by blending into magnetite concentrates, as reported in authors' earlier work.^[4] In comparison, oxidation of magnetite spinel phase has no obvious shift of both (220) and (104) peak positions within the whole temperature range.

The large discrepancy of the oxidation process between chromite and magnetite spinels is mostly attributed to their different state of Fe^{2+} ions in spinel crystals. Magnetite has an inverse spinel structure in which Fe^{2+} ions locate on the octahedral sites (B sites) while chromite has a normal spinel structure with Fe^{2+} ions distributed on the tetrahedral sites (A sites).^[35] And



(a)



(b)

Fig. 10—Effect of preheating (a) and roasting (b) temperatures on the compressive strength of chromite and magnetite pellets.

a considerable number of work has suggested that the tetrahedral interstices are smaller than the octahedral ones in spinel-type oxides and hence leading to minor diffusion mobility of A site cations.^[36,37] Besides, more recent studies concerning the point defects and cation diffusion in iron-bearing spinel crystals have been conducted theoretically by applying the hybrid functional method, molecular dynamics (MD) simulations, or computer modeling,^[38,39] and experimentally using electrochemical method, cation tracer diffusion method, and Mössbauer study.^[8,12,40,41] All this confirms better mobility of Fe^{2+} in magnetite spinel than that in chromite spinel. In addition, oxidation of magnetite in air is controlled by efficient vacancy diffusion through the octahedral sites while oxidation of chromite spinel is likely to be a combined result of both interstitial and vacancy diffusion on the tetrahedral sites.

C. Oxidation Kinetics of Chromite and Magnetite Pellets

The curves of oxidation extent x vs time t for chromite pellets and magnetite pellets conducted at different temperatures are shown in Figures 7(a) and (b). It can

be observed that the oxidation of magnetite pellets is much faster than that of chromite pellets in the whole temperature range. After oxidized at 1223 K for 10 minutes, the oxidation extent of magnetite pellet reaches over 90 pct while chromite pellet can only reach about 60 pct.

Aforementioned model formulas, *i.e.*, Eqs. [3] through [6] were applied to fit the kinetic data of the initial stage featured with high oxidation rate, as shown in Figure 8. The best linear fit is found in the case of rate controlled by chemical reaction, $F_p = F_g = 3$. For the sake of simplicity, rate controlled by both chemical reaction and diffusion were not demonstrated in the figure because of the evidently poor fit. Reaction rate constants (k) of the pellets at different temperatures are the slopes of corresponding straight lines, as given in Table IV. The relationship between $\ln k$ and $1/T$, as shown in Figure 9, also suggests an excellent linear relation. By applying Eq. [7], the apparent activation energies (E_a) for oxidation of chromite and magnetite pellets from 1073 K to 1223 K (800 °C to 950 °C) can be calculated, *i.e.*, 65.74 and 38.74 kJ/mol, respectively. The measured apparent activation energies seem to be

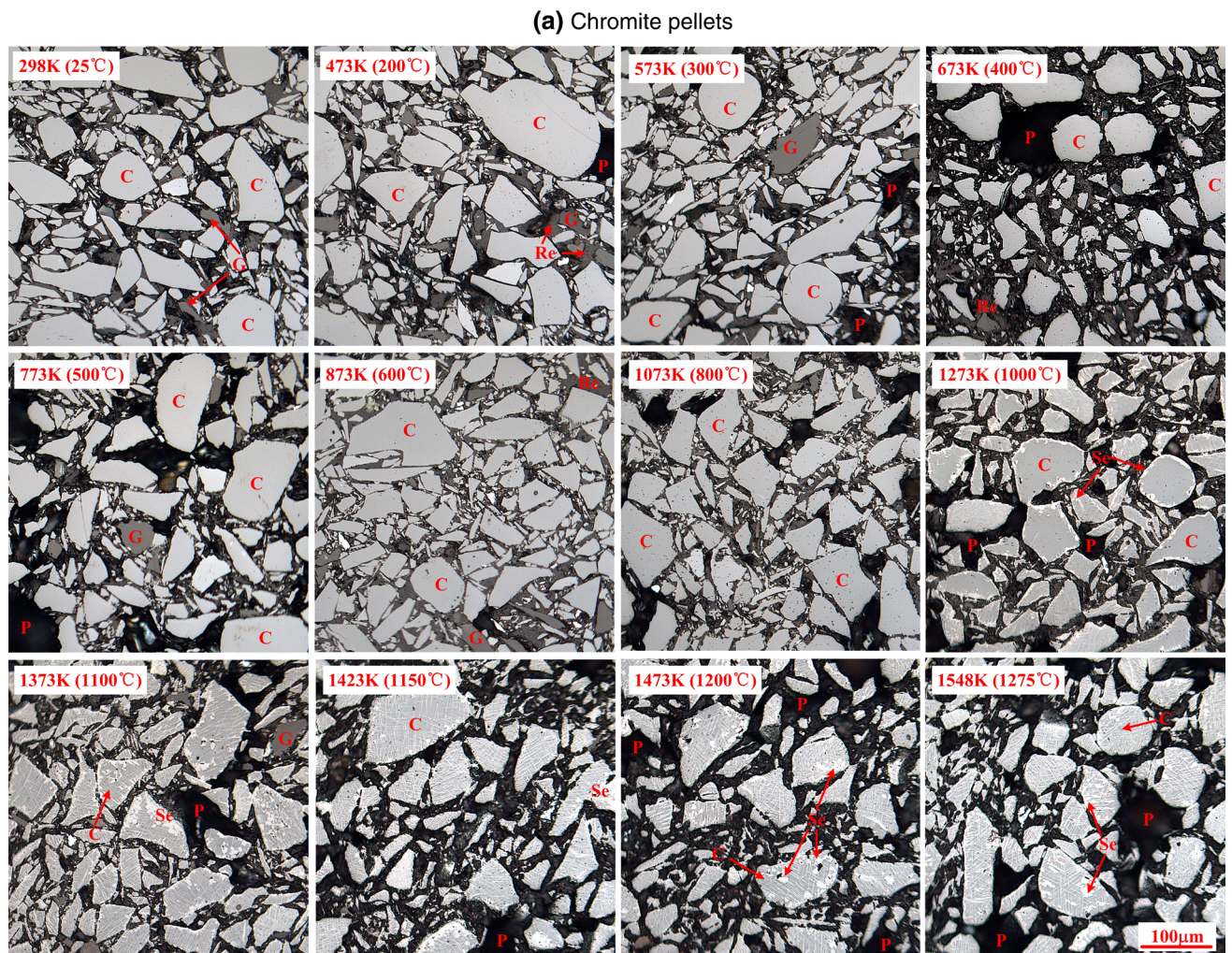


Fig. 11—The microstructure of preheated and roasted chromite and magnetite pellets, labels: C-chromite spinel; Se-sesquioxide; M-magnetite spinel; H-hematite; G-gangue; P-pore; Re-resin.

(b) Magnetite pellets

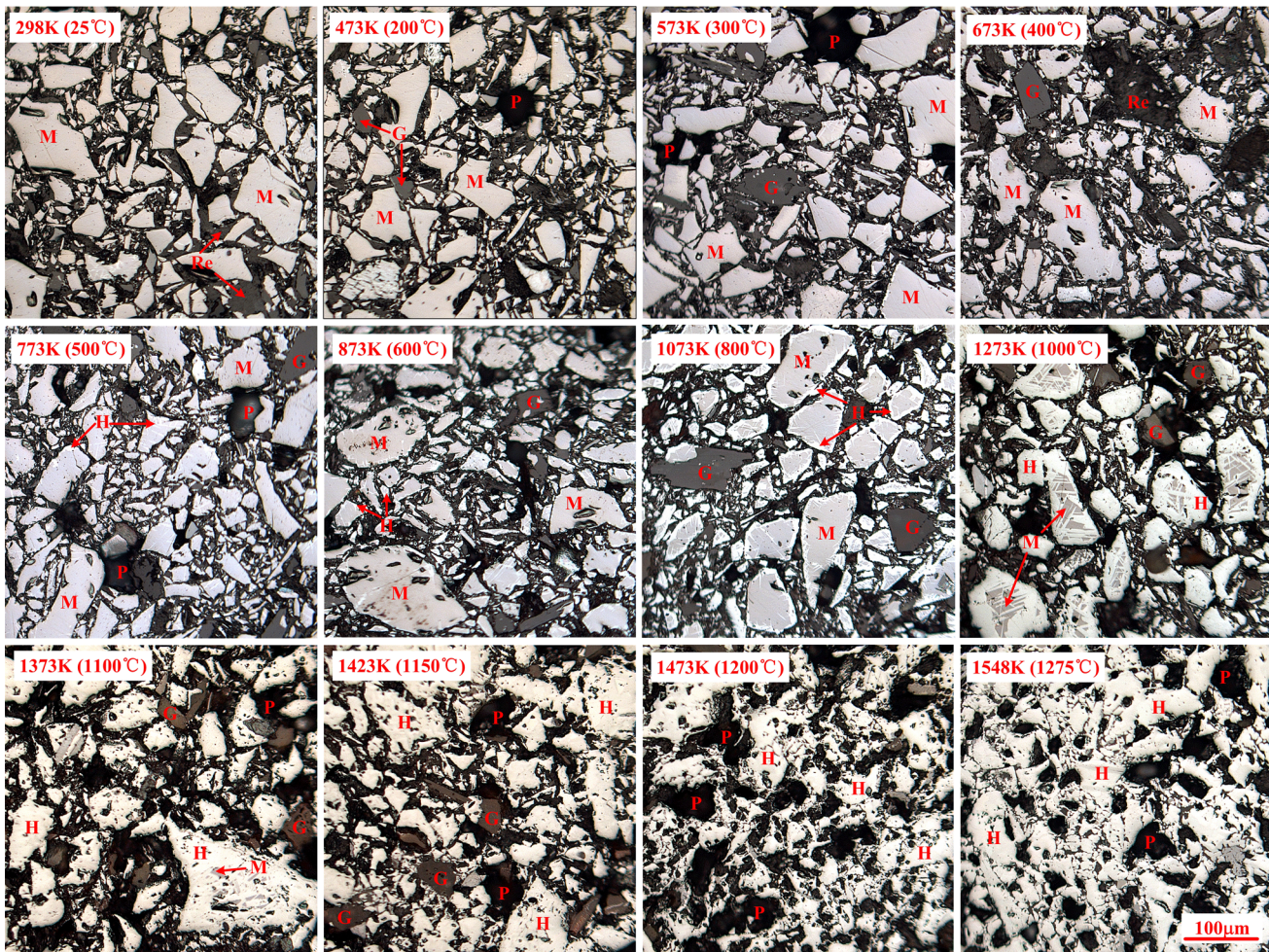


Fig. 11—continued.

reasonable compared with previous literatures.^[5,12,24,42] It can be revealed that oxidation of chromite needs more activation energy than that of magnetite.

D. Preheating–Roasting Performance of Chromite and Magnetite Pellets

The above discussions have shown the distinct oxidation behaviors of chromite and magnetite from the viewpoint of thermodynamics and dynamic kinetics. To further reveal the effect of oxidation behavior of ferrous raw materials on the microstructure and consolidation of their pellets, relevant investigations on the preheating–roasting performance of dried chromite and magnetite pellets were conducted. The compressive strength of preheated chromite and magnetite pellets from room temperature to 1373 K (1100 °C) as well as their fired pellets is shown in Figures 10(a) and (b), respectively. And the microstructure of preheated and roasted chromite and magnetite pellets at different temperatures is demonstrated in Figures 11(a) and (b).

Two pellets bear almost the same inherent compressive strength, as can be depicted from Figure 10(a), and low-temperature oxidation below 623 K (350 °C) seems

to have little impact on their mechanical strength. Then initial but very limited strength gain appears at above 673 K (400 °C) for both pellets, which possess similar strength up to 823 K (550 °C). The solid-state reactions and surface oxidation of chromite and magnetite spinel help form initial bridging among particles, which may account for the increase in pellet strength. When preheating temperature reaches over 873 K (600 °C) until 1173 K (900 °C), the chromite pellet has a faster increase in its compressive strength than magnetite pellet, in contradiction to their oxidizability. This may be caused by the combined effect of magnetite core shrinking and possible particle deterioration at elevated temperatures due to the inferior thermal stability of magnetite spinel than chromite spinel, as can be revealed from Figures 11(a) and (b).^[43–45] Then the compressive strength of preheated chromite pellet undergoes a slow increase in the temperature range of 1173 K to 1373 K (900 °C to 1100 °C), even under roasting conditions, as shown in Figure 10(b). According to the phase analysis, the formation of Fe-rich sesquioxide reaches a high extent after preheating at below 1173 K (900 °C) corresponding to the rapid increase of compressive strength and thereafter undergoes the formation of

Cr-rich sesquioxide within the chromite particle and poor consolidation of mineral particles. This point of view can be further explained by the microstructure of two pellets in Figure 11. The formation and recrystallization of sesquioxide in chromite pellet is very limited. In contrast, the compressive strength of preheated magnetite pellet increases drastically with the temperature rise due to the recrystallization of hematite and efficient sintering of the particles at high temperatures. The compressive strength of magnetite pellet at 1548 K (1275 °C) can reach nearly 3000 N per pellet, whereas that of chromite pellet can only reach about 1300 N per pellet. The microstructure of two pellets is in good correspondence to the thermal and phase analysis, showing that the consolidation of oxidized ferrous pellets is largely affected by the inherent oxidation behavior of iron-bearing raw materials.

IV. CONCLUSION

The oxidation behavior of high FeO chromite and chromite ores in air and its relevance to the consolidation of their pellets were revealed in this work by fundamentally investigating their thermal properties, phase transformation, oxidation kinetics, and preheating-roasting performance. Any single technique seems insufficient to characterize the unambiguous oxidation mechanism of chromite and magnetite spinels at elevated temperatures because of the considerable overlapping effect of oxidation, phase and magnetic transition, and recrystallization. But both thermal and phase analyses show the evidence that the oxidizability of chromite spinel is inferior to that of magnetite. More specifically, oxidation of high FeO chromite spinel always accompanies the preferential formation of Fe-rich sesquioxide at low temperatures and thereafter a Cr-rich sesquioxide forms on the Fe-rich substrate at high temperatures. The oxidation kinetics of chromite and magnetite pellets in the temperature range of 1073 K to 1223 K (800 °C to 950 °C) reveal that their apparent activation energies are 65.74 and 38.74 kJ/mol, respectively. The distinct inherent oxidation behaviors of chromite and magnetite concentrates are proved to have a large effect on the induration process of their oxidized pellets. This work has suggested the importance of smart ore blending of chromite and iron ore concentrates in manufacturing high quality chromium-bearing pellets. Other effects such as particle size distribution, mechanical activation, and the presence of gangue all may affect the oxidizability of raw materials and the consolidation of pellet and will be our future work.

ACKNOWLEDGMENTS

The authors are thankful for financial supports from the National Science Foundation of China (No. 51474161) and Hunan Provincial Co-innovation

Center for Clean and Efficient Utilization of Strategic Metal Mineral Resources. The authors also wish to express their gratitude to the School of Materials Science and Engineering in Central South University, which provides the facilities to do the measurements.

REFERENCES

1. L.A. Cramer, J. Basson, and L.R. Nelson: *J. S. Afr. I. Min. Metall.*, 2004, vol. 104, pp. 517–27.
2. J. Daavittila, M. Honkaniemi, and P. Jokinen: *J. S. Afr. I. Min. Metall.*, 2004, vol. 104, pp. 541–9.
3. D.Q. Zhu, C.C. Yang, J. Pan, and Y. Zhong: in *6th International Symposium on High-Temperature Metallurgical Processing*, T. Jiang, J.Y. Hwang, G.R.F.A.F.O. Yücel, X. Mao, H.Y. Sohn, N. Ma, P.J. Mackey, and T.P. Battle, eds., Wiley, Hoboken, NJ, 2015, p. 139.
4. D.Q. Zhu, C.C. Yang, J. Pan, Q. Zhang, B.J. Shi, and F. Zhang: *Metall. Mater. Trans. B*, 2016, vol. 47B, pp. 1010–23.
5. D. Papanastassiou and G. Bitsianes: *Metall. Mater. Trans. B*, 1973, vol. 4B, pp. 487–96.
6. J.R. Wynnyckyj and T.Z. Fahidy: *Metall. Trans.*, 1974, vol. 5, pp. 991–99.
7. Y.M. Zhang: *Theory and Technology of Iron Ore Pelletizing*, 1st ed., Metallurgical Industrial Press, Beijing, 1997, pp. 95–130 (in Chinese).
8. B. Gillot, R.M. Benloucif, and F. Jemmal: *J. Mater. Sci.*, 1984, vol. 19, pp. 3806–13.
9. B. Gillot and F. Jemmal: *J. Mater. Sci.*, 1986, vol. 21, pp. 4436–42.
10. J.P. Sanders and P.K. Gallagher: *Thermochim. Acta*, 2003, vol. 406, pp. 241–43.
11. E.R. Monazam, R.W. Breault, and R. Siriwardane: *Lnd. Eng. Chem. Res.*, 2014, vol. 53, pp. 13320–28.
12. B. Gillot, J.F. Ferriot, G. Dupré, and A. Roussat: *Mater. Res. Bull.*, 1976, vol. 11, pp. 843–49.
13. B. Gillot, F. Bouton, and F. Chassagneux: *Mater. Res. Bull.*, 1980, vol. 15, pp. 1–7.
14. S. Sarkar and J. Ghose: *J. Therm. Anal.*, 1990, vol. 36, pp. 2593–99.
15. J.M.G. Amores, V.S. Escibano, and G. Busca: *Mater. Chem. Phys.*, 1999, vol. 60, pp. 168–76.
16. V.D. Tathavadkar, M.P. Antony, and A. Jha: *Metall. Mater. Trans. B*, 2005, vol. 36B, pp. 76–84.
17. S.S. Ramos, A.D. Carbó, J.G. Adelantado, J.P. Vicente, and F.M. Algarra: *Thermochim. Acta*, 2008, vol. 476, pp. 11–19.
18. X.L. Liang, Y.H. Zhong, S.Y. Zhu, H.P. He, P. Yuan, J. Zhu, and J. Zheng: *Solid State Sci.*, 2013, vol. 15, pp. 115–22.
19. Y.W. Li: *Ph.D Dissertation*, Shanghai University, 2010, p. 174–77 (in Chinese).
20. D.Q. Zhu, Y.H. Luo, J. Pan, and W.T. Zhou: *Metal Mine*, 2011, pp. 89–93 (in Chinese).
21. G.Z. Qiu, D.Q. Zhu, J. Pan, C.A. Wang, Y.F. Guo, T. Jiang, C.F. Hu, J. Clout, and F.H. Shu: *ISIJ Int.*, 2004, vol. 44, pp. 69–73.
22. J. Szekeley, J.W. Evans, and H.Y. Sohn: *Gas-solid Reactions*, 3rd ed., Academic Press, New York, 1976, pp. 73–104.
23. J.Y. Fu, Y.T. Li, C.W. Jiang, and L.Q. Wang: *J. Cent. South Univ. (Science and Technology)*, 2004, vol. 35, pp. 950–54 (in Chinese).
24. R.Q. Liang, S. Yang, F.S. Yan, and J.C. He: *J. Iron Steel Res. Int.*, 2013, vol. 20, pp. 16–20.
25. H.Q. Tang, X.M. Guo, S.B. Zhang, and Z.C. Guo: *J. Iron Steel Res.*, 2000, vol. 12, p. 1 (in Chinese).
26. J.H. Liu, J.Y. Zhang, and T.P. Zhou: *J. Iron Steel Res.*, 2000, vol. 34, p. 5 (in Chinese).
27. E.R. Schemidt and F.H.S. Vermaas: *Am. Mineral.*, 1955, vol. 40, pp. 422–31.
28. A.C.D. Chaklader and G.R. Blair: *J. Therm. Anal.*, 1970, vol. 2, pp. 165–79.
29. J.P. Sanders and P.K. Gallagher: *J. Therm. Anal. Calorim.*, 2003, vol. 72, pp. 777–89.

30. R.G. Richards and J. White: *Trans. Br. Ceram. Soc.*, 1954, vol. 53, pp. 233–70.
31. H. Schmalzried: *Chemical Kinetics of Solids*, VCH, Cambridge, 1995, pp. 19–42.
32. K. Huang: *Solid State Physics*, Peking University Press, Beijing, 2013, pp. 60–80 (in Chinese).
33. C. Kittel: *Introduction to Solid State Physics*, Wiley, Hoboken, NJ, 2005, pp. 584–618.
34. P.K. Gallagher, E.M. Gyorgy, and H.E. Bair: *J. Chem. Phys.*, 1979, vol. 71, pp. 830–35.
35. M.D. Osborne, M.E. Fleet, and G.M. Bancroft: *Contrib. Mineral Petrol.*, 1981, vol. 77, pp. 251–55.
36. R. Sun: *J. Chem. Phys.*, 1958, vol. 28, pp. 290–93.
37. J.S. Armijo: *Oxid. Met.*, 1969, vol. 1, pp. 171–98.
38. J. Vaari: *Solid State Ionics*, 2015, vol. 270, pp. 10–17.
39. A.A. Yaremchenko, A.V. Kovalevsky, E.N. Naumovich, V.V. Kharton, and J.R. Frade: *Solid State Ionics*, 2011, vol. 192, pp. 252–58.
40. J. Töpfer, S. Aggarwal, and R. Dieckmann: *Solid State Ionics*, 1995, vol. 81, pp. 251–66.
41. K.D. Becker and V.V. Wurm: *Hyperfine Interact.*, 1990, vol. 56, pp. 1431–36.
42. Z.Q. Song: *Master thesis*, Central South University of Technology, 2000, pp. 27–48 (in Chinese).
43. J.R. Wynnycyk and W.A. McCurdy: *Metall. Trans.*, 1974, vol. 5, pp. 2207–15.
44. S.P.E. Forsmo, S.E. Forsmo, P.O. Samskog, and B.M.T. Björkman: *Powder Technol.*, 2008, vol. 183, pp. 247–59.
45. V. Strezov, T.J. Evans, V. Zymła, and L. Strezov: *Int. J. Miner. Process.*, 2011, vol. 100, pp. 27–32.